ICES Journal of Marine Science, 2022, **79**, 648–660
DOI: 10.1093/icesjms/fsac006
Advance access publication date: 8 February 2022
Original Article

Aerial detection of beached marine plastic using a novel, hyperspectral short-wave infrared (SWIR) camera

Jennifer Cocking [1,*], Bhavani E. Narayanaswamy [1], Claire M. Waluda [2] and Benjamin J. Williamson [3]

[1]Scottish Association for Marine Science, University of the Highlands and Islands, Oban PA37 1QA, UK
[2]British Antarctic Survey, Natural Environment Research Council, Cambridge CB3 0ET, UK
[3]Environmental Research Institute, North Highland College, University of the Highlands and Islands, Thurso KW14 7EE, UK
[*] *Corresponding author: tel:+44 (0)1631 559000;* e-mail: jennifer.cocking@sams.ac.uk.

Plastic pollution in the marine environment is a pervasive, global problem that threatens wildlife and human health. Routine monitoring is required to determine pollution hotspots, focus clean-up efforts, and assess the efficacy of legislation implemented to reduce environmental contamination. The shoreline represents an accessible area, relative to open water, from which to monitor this. Unmanned aerial vehicles (UAVs) offer a low-cost platform for remote sensing that operates below cloud coverage, which can interfere with satellite imagery. Detection of plastic using visible light is limited however, and results may be improved by using short-wave infrared (SWIR) imagery to collect chemical information. Within the commercial recycling industry, plastic items are sorted successfully based on their composition using SWIR instrumentation that measures the chemical spectra of waste items under controlled illumination. Here, proof of concept is established for aerial detection of domestic and shoreline-harvested plastic items on a beach under natural sunlight with a lightweight (800 g), hyperspectral SWIR camera deployed at an altitude of ∼ 5 m over ∼ 30-m transects. The results of spectral correlation mapping to compare imagery spectra to polyethylene and polypropylene reference spectra demonstrate that these two polymers can be successfully detected with this novel method.

Keywords: hyperspectral, macroplastics, plastic pollution, remote sensing, shoreline, short-wave infrared, spectral angle mapping.

Introduction

Plastic pollution continues to accumulate in the marine environment due to ever-increasing human activity and the production and consumption of plastic items—on the order of millions of metric tons each year (Jambeck *et al.*, 2015; Law *et al.*, 2020). The already observed consequences include wildlife entanglement and ingestion by wildlife of plastics of various size (Gall and Thompson, 2015; Van Franeker and Law, 2015; Avio *et al.*, 2017; Phillips and Waluda, 2020). Negative impacts are also anticipated regarding human health, with the observation of microplastics (< 5 mm) in species fished for human consumption, as well as in other food items and beverages (CONTAM, 2016). Macroplastics (> 5 mm), in addition to entanglement risks, are a significant source of microplastics. This is especially true for beached macroplastics that encounter greater exposure to ultraviolet (UV) light and oxygen than waterborne plastics, as well as often greater temperatures, all of which promote embrittlement and fragmentation (Andrady, 2011; GESAMP, 2015).

Researchers have developed methods of observing, collecting, and measuring plastic pollution as diverse as the environments in which it is found: shoreline surveys (Melvin *et al.*, 2021), net tows in surface waters (Law *et al.*, 2014), vessel intake pumps below the water's surface (Cincinelli *et al.*, 2017), sediment cores, and extraction from dissected biota (Mai *et al.*, 2018). Many of these individual methods present challenges including subjectivity and effort bias, physical sample storage, destructive analysis techniques, and limited time and financial resources that restricts sampling opportunities and coverage. Researchers studying different environments or working in different groups use different methodological parameters and units of measurement to record observations and report results (Waller *et al.*, 2017; Boucher and Billard, 2019). This inconsistency can limit the comparison of findings and consequently, the strength of evidence-based recommendations to support policy changes regarding the use, management, and environmental/health impacts of plastic materials. The need for data standardization has represented a key topic of discussion at various scientific meetings within the field of plastic pollution research (Kershaw *et al.*, 2019).

Remote sensing (RS) provides an opportunity for objective, efficient, and scalable observation/monitoring of plastic pollution. Studies using imagery collected by satellite, manned aircraft, and unmanned aerial vehicles (UAVs) have reported preliminary success in detecting plastic in the marine environment (Garaba and Dierssen, 2018; Biermann *et al.*, 2020; Balsi *et al.*, 2021; Freitas *et al.*, 2021). UAVs complement the two higher-altitude platforms, as they operate below the interference of cloud. UAVs are also more economical, more readily accessible, and provide additional opportunity to access locations that may be prohibitive to manned flight due to any combination of logistics, resources, and safety.

Received: August 2, 2021. **Revised:** December 15, 2021. **Accepted:** December 17, 2021

Plastic materials have characteristic absorption features throughout the infrared (IR) spectrum that enable their detection. These features provide chemical information and can strongly support identification of the material, rather than relying solely on colour and geometric information captured by conventional visible imagery. The IR spectrum is divided into multiple regimes, defined by different wavelength ranges depending upon field of study and, within the field of RS, sensor specifications. To contextualize this research, we define these IR regimes as: near-infrared (NIR) 0.7–1.0 μm; short-wave infrared (SWIR) 1–3 μm; mid-wave infrared (MWIR) 3–5 μm; and long-wave infrared (LWIR) 7–14 μm. These regimes agree approximately with those summarized by Peckham *et al.* (2015).

Fourier Transform Infrared (FTIR) spectroscopy is a common method of characterizing plastic samples in the laboratory (Renner *et al.*, 2017a). This technique uses an active source of IR light, which spans the MWIR to LWIR regimes. Numerous studies regarding the detection of plastic debris in the environment have confirmed, however, that water (including that in Earth's atmosphere) strongly absorbs and attenuates LWIR energy. Mace (2012) indicated that IR penetration is generally limited beyond the top few millimetres of the water column. Veenstra and Churnside (2012) specifically emphasized that the penetration of the water column by LWIR energy is limited to approximately 10 μm for wavelengths of 7–14 μm and in application, the specified spectral range did not yield good results for detecting abandoned fishing nets. LWIR would require debris to be floating at the very surface of the sea and for its temperature to contrast sufficiently with the bulk background of the water. Goddijn-Murphy and Williamson (2019) reported that the difference in temperature between the water surface and its surroundings was indeed key to the RS of floating plastic litter with thermal IR (comprising MWIR and LWIR).

The recycling industry successfully sorts plastic materials based on resin type by exploiting absorption features in the SWIR regime (Masoumi *et al.*, 2012). A greater amount of SWIR energy emitted by the sun reaches Earth's surface than LWIR, and SWIR energy penetrates water to a greater extent (up to ∼ 3 cm) than LWIR (less than 0.01 cm; Peckham *et al.*, 2015). Daylight, therefore, offers passive illumination for the purpose of plastic detection in the outdoor environment using SWIR. Some SWIR wavelengths are more strongly absorbed by the atmosphere and are not as useful as others for RS. Garaba and Dierssen (2018) highlight that atmospheric absorption especially impacts SWIR reflectance within the ∼1300–1500 nm range. Within the remainder of the SWIR regime, common plastic resins exhibit characteristic absorption features at bands including ∼1200 and ∼1700 nm, useful for RS of plastic (Masoumi *et al.*, 2012; Garaba and Dierssen, 2018).

Spectral angle mapping (SAM) is a technique to determine the similarity of spectra to one another, based on the cosine similarity, which describes the angle between two vectors (Kruse *et al.*, 1993). The SAM algorithm is commonly applied to hyperspectral data cubes to differentiate and classify pixels of different materials within an image, based on a set of reference spectra. Bogfjellmo (2016) and Garaba and Dierssen (2018) each used SAM to characterize plastic objects by their spectral features in the ranges of 1000–2500 nm and 350–2500 nm, respectively. Bogfjellmo (2016) observed that with respect to two other methods—Principal Component Analysis (PCA) and Partial Least Squares Discriminant Analysis—SAM yielded the most consistent classification results. Bogfjellmo (2016) indicated that PCA is very sensitive to varying illumination, while SAM treats different illuminations equally and is insensitive to gain. SAM is also independent of linear scaling i.e. the magnitude of compared vectors does not influence the angle between them. Kulcke *et al.* (2003) also concluded that SAM achieved the best polymer classification results (in the range of 1000–1700 nm), against three other methods (the Linear and Quadratic Discriminant Classifiers and the Fisher Linear Discriminant Classifier).

Spectral Correlation Mapping (SCM) is a variant of SAM, based on the Pearson Correlation Coefficient. SCM differs from SAM, in that the compared vectors are centred by their respective means. De Carvalho and Meneses (2000) demonstrated the difference in outcome of applying SAM and SCM on artificial spectra, and proposed SCM as an improvement over SAM due to its ability to capture negative spectral correlations. Shivakumar and Rajashekararadhya (2017) achieved better overall classification in a land mapping study with SCM (73.00% accuracy) than with SAM (69.56% accuracy).

Researchers have only recently begun to investigate the feasibility and efficacy of detecting plastic in the natural environment with SWIR sensors. SWIR absorption features have been used to identify terrestrial synthetic hydrocarbons in airborne visible-infrared imaging spectrometer (AVIRIS) imagery (Garaba and Dierssen, 2018), as well as floating ocean plastics in SWIR imagery collected via manned aircraft within the "Great Pacific Garbage Patch" (Garaba *et al.*, 2018). Biermann *et al.* (2020) applied one of Sentinel 2's SWIR imaging bands to develop a satellite-based "floating debris index" with a reported plastic classification accuracy of 86% against the environmental background and within natural, floating materials. Freitas *et al.* (2021) achieved 70–80% precision in the detection of three different types of floating plastic targets (10 × 10 m) in hyperspectral SWIR images captured from a manned aircraft (600 m altitude). Freitas *et al.* (2021) also demonstrated that flight altitude did not meaningfully impact the spectral response absorption bands of plastic targets, by comparing the spectral data captured at 600 m to that captured by the same imaging system deployed with a UAV at altitudes between 20 and 35 m. At ground level, Goddijn-Murphy and Dufaur (2018) evaluated a dual-band NIR/SWIR algorithm to model light reflectance of plastics floating on natural waters, reporting that measured reflectance was highly dependent upon the chemical and physical properties of the plastic items. The authors concluded that it was not possible to use a singular RS algorithm to quantify plastic litter floating on natural waters from reflectance data alone (Goddijn-Murphy and Dufaur, 2018).

Shoreline accumulation is a significant fate for waterborne plastics and represents a key observational scenario (Martinez-Vicente *et al.*, 2019). From their mass balance model, Lebreton *et al.* (2019) estimated that the world's shorelines store approximately 67% of all buoyant macroplastic—millions of metric tons—released into the marine environment since the 1950s. SWIR instrumentation offers potentially even greater detection capability in a shoreline application relative to water-based observation, given the attenuation of SWIR by water. In comparing the spectral reflectance of dry and wet microplastics measured outdoors, Garaba and Dierssen (2018) demonstrated decreased SWIR reflectance of

approximately 90% for the wet microplastics. Researchers have studied beached plastic accumulation with aerial image capture and processing techniques including high resolution RGB imagery and digital supervised classification (Acuña-Ruz *et al.*, 2018), and photogrammetry with manual image screening (Duarte *et al.*, 2020; Andriolo *et al.*, 2021a, b). Freitas *et al.* (2021) references additional studies implementing UAV-based RGB image capture for the detection of plastic debris. There are limited studies, however, that have applied SWIR imaging techniques to the detection of *in situ* shoreline plastic. Recently, Guffogg *et al.* (2021) demonstrated that the bulk reflectance SWIR spectra (measured with a handheld spectroradiometer) of some sandy beach quadrats containing plastic items were statistically different from those not containing any plastic. Balsi *et al.* (2021) reported successful detection of plastic materials (on shore and floating in seawater) in hyperspectral SWIR imagery collected by UAV and analysed with Linear Discriminant Analysis for similarity to polyethylene and polyethylene terephthalate reference spectra.

The aim of this study is to strengthen and expand upon existing research that supports the feasibility of automated RS of shoreline plastic debris by hyperspectral SWIR imaging (Garaba and Dierssen, 2018; Martinez-Vicente *et al.*, 2019; Balsi *et al.*, 2021; Guffogg *et al.*, 2021). The presented methodology implements and tests an instrument and platform that is low-cost and lightweight for the intended application of collecting imagery from a UAV at much lower altitudes than manned aircraft and satellites. This study explores the detection of plastic as a general material class with additional focus specifically on detecting polyethylene (PE) and polypropylene (PP), which are the most commonly produced resins and the most abundant in the environment (ter Halle *et al.*, 2017; Renner *et al.*, 2017b).

Material and methods

Sample items

Plastic sample items were harvested from both domestic (20 items) and natural environments (46 items). These collections included samples of (in order of numerical resin code) polyethylene terephthalate (PET), high density polyethylene (HDPE), polyvinyl chloride (PVC), low density polyethylene (LDPE), PP, polystyrene (PS), expanded polystyrene (EPS), acrylonitrile butadiene styrene (ABS), polylactic acid (PLA), and nylon 6, all verified by FTIR spectroscopy in attenuated total reflectance mode (ATR–FTIR). An additional melamine item (ash tray) could not be verified by FTIR—the composition is assumed, as melamine is commonly used to produce ash trays because of its flame retardancy.

Preliminary hyperspectral SWIR image collection was performed with the domestic items, as well as two PP ropes, one fragment each of PE and PP, two fragments of EPS, and a PLA takeaway cup lid—all seven of which were collected from the shoreline. This preliminary assortment is described in Table 1. Additional items harvested from the natural environment were subsequently gathered to support performance comparison of detection of domestic plastic items and beached/littered plastics. The environmentally sourced assortment is described in Table 2.

Hyperspectral SWIR camera instrumentation

Images of the plastic items were collected with a BaySpec (San Jose, CA) OCI-F SWIR hyperspectral pushbroom camera (mass 800 g), measuring reflectance in 36 wavelengths between 900 and 1700 nm (with band intervals between 15.4 and 26.6 nm, and an average band interval of 21.1 nm). The camera comprises two sensors behind the singular, 16 mm lens: the pushbroom SWIR sensor (resolution of 250 pixels ×

Table 1. Preliminary assortment of plastic sample items, harvested from the domestic (20 items) and the natural environment (seven items), for spectral measurement with a SWIR camera. ∗ indicates items collected from the natural environment.

Resin	Total items	Pieces	Description	Colour
PET	7	1	Square 5 L bottle	Colourless, label one side
		1	Round 5 L bottle	Colourless with wraparound label
		1	2 L bottle	Colourless with wraparound label
		1	Drink bottle	Colourless with wraparound label
		1	Washing up liquid bottle	Colourless, label one side
		2	Produce containers	Colourless
PE	5	1	LDPE bag	Colourless
		1	HDPE milk bottle	White
		1	HDPE supplement bottle	Silver
		1	HDPE bottle caps (3 grouped)	Red, green, and blue
		1	HDPE fragment∗	Grey
PP	10	1	Fragment∗	Dark blue
		1	Disposable flat spoon	Dark blue
		2	Tub and lid	White
		2	Tub and lid	Colourless
		2	Cylindrical bottles	Off-white
		2	Ropes∗	Blue
EPS	3	2	Fragments∗	White
		1	Peanuts (3 grouped)	Light green
ABS	1	1	Disc (back cover of smoke detector)	Off-white
PLA	1	1	Takeaway cup lid∗	White
Total	27			

Table 2. Assortment of plastic sample items collected from the natural environment, for spectral measurement with a SWIR camera.

Resin	Total items	Pieces	Description	Colour
PET	8	4	Bottles	Colourless, no labels
		1	Bottle	Colourless, no label, heavy fouling
		1	2 L bottle	Colourless with wraparound label
		1	Drink bottle	Purple with fouling
		1	Reusable drinking pouch	Yellow and brown
PE	10	1	HDPE bottle	Green, no label
		1	HDPE bottle	Yellow, no label
		1	HDPE jug	White
		1	HDPE can	Green
		1	HDPE barrel lid	Black
		1	HDPE crab bait container	Coral
		1	HDPE sealant tube	White and beige, black text
		1	HDPE fragment	Black
		1	HDPE rectangular tube	Dark blue
		1	LDPE bottle	Red
PVC	3	1	Boat fender buoy	White with dark blue ends
		1	Boat fender buoy	White with fouling
		1	Pool float	Light blue
PP	7	1	Bucket lid	White
		1	Seat portion of chair	White
		1	Seat fragment	Colourless, some scorching
		1	Beach toy, shovel, no handle	Blue
		1	Beach toy, sand mould	Orange
		2	Langoustine box inserts	White
PS	5	1	Confectionary gift box	Colourless
		1	Takeaway cup lid	White
		1	Single-use cup	Red
		2	Single-use cups	Colourless
PE/PP blend	4	2	Ropes	Teal
		1	Rope	White with fouling
		1	Glove	Orange with fouling
Nylon 6	1	1	Large bag	Colourless
Melamine (not confirmed by FTIR)	1	1	Ash tray	Black
Total	**39**			

scan length) as well as a snapshot sensor that collects visible light to produce interpretable monochrome reference images. Each sensor was powered through a USB connection to an Intel Compute stick (STK2M3W64CC), which also stored the collected images. The portable configuration was powered by lithium polymer batteries via a DC/DC converter and an actively powered USB 3.0 hub. Peak consumption is 50 W, with a typical consumption of < 10 W, according to BaySpec's manual for the camera. A sunlight readable touch screen display was connected to the computer's HDMI port to operate the camera with BaySpec's SpecGrabber software. Exposure was set automatically according to the environmental background and fixed prior to image and reference collection. Reference images were collected of the manufacturer-supplied white reference (95% reflectance) and dark reference images were collected with the lens cap fully covering the camera's foreoptic.

Camera deployment and image collection

Plastic items were placed along dry sandy regions of the shoreline (above the seaweed strand line) adjacent to the Scottish Association for Marine Science in Oban, Scotland (approximately 56°27′11″N 5°26′35″W).

Images of each plastic item in the preliminary assortment (Table 1) were first captured individually to collect spectral data such that image regions containing plastic spectral signal were easily discernible by visual inspection. The camera was held at waist height at a 0° nadir angle, approximately 1 m above the plastic targets that had been pre-arranged on the sand and the camera was manually moved forward at arm's length to collect images of these individual items.

To investigate the collection of aerial data, the camera was attached to a taut line strung at a level height of approximately 5 m above the beach, between a natural feature on the shoreline and the top of a telescopic mast. The mast was secured with three lines temporarily anchored in the ground. A custom camera trolley was used to convey the camera across the approximately 30-m-long transect line (Figure 1). White and dark references were captured, and image capture was started with a delay before disconnecting the display, feeding the trolley on to the line, and securing the free end of the line to a natural anchor point. The camera trolley was pulled steadily across the highline at approximately 0.3 m/s (to minimize vibration/sway) with a lightweight line to capture images of plastic items in each assortment, arranged in a linear transect on the sand below. Images of the preliminary assortment

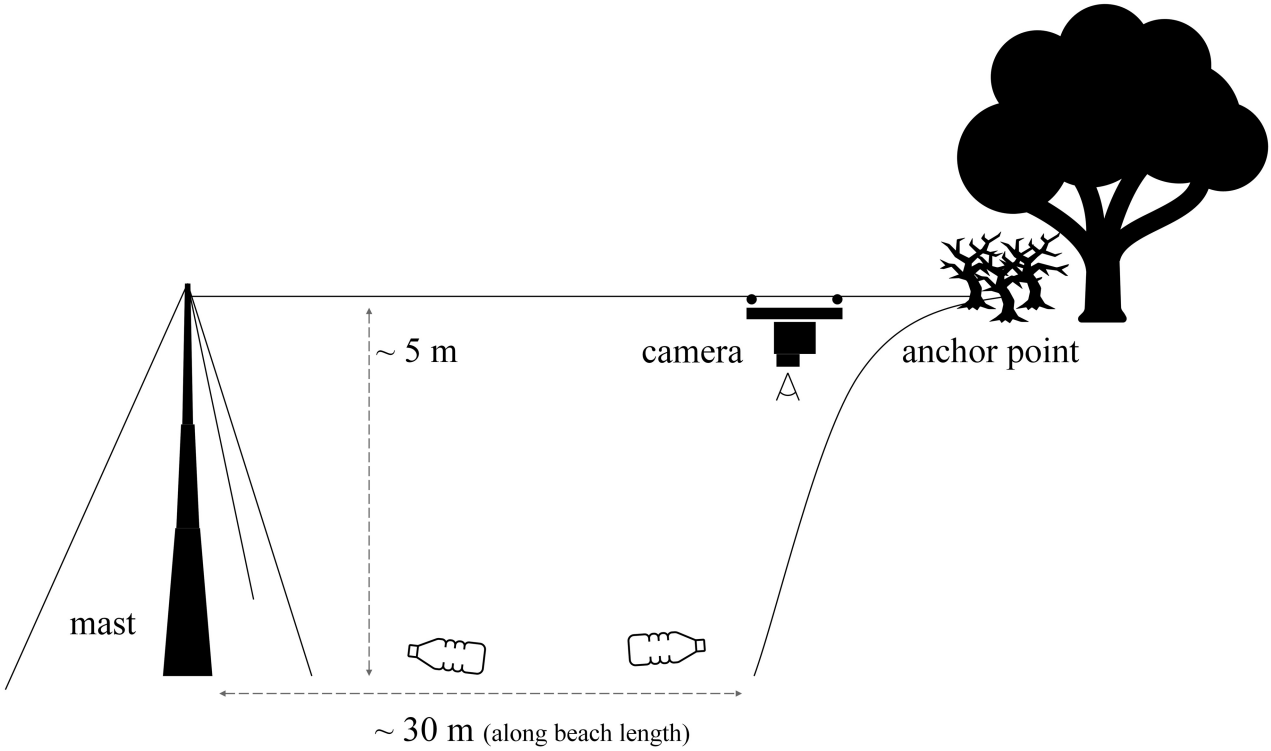

Figure 1. Schematic of hyperspectral SWIR camera deployment on a highline to collect aerial images of plastic items arranged in a linear transect on the shoreline (not to scale).

were collected on 29 November 2019 and the environmentally sourced assortment on 18 September 2020. Both days were sunny with negligible cloud. All images were collected within 2 h of midday, targeting maximum sun angle.

Data processing and spectral comparison

Individual collected frames were stitched together to create an image of each full plastic item or beach transect with BaySpec's CubeCreator software. No spectral binning was applied to the 36 measured bands. MATLAB was used for all subsequent processing of hyperspectral cube data.

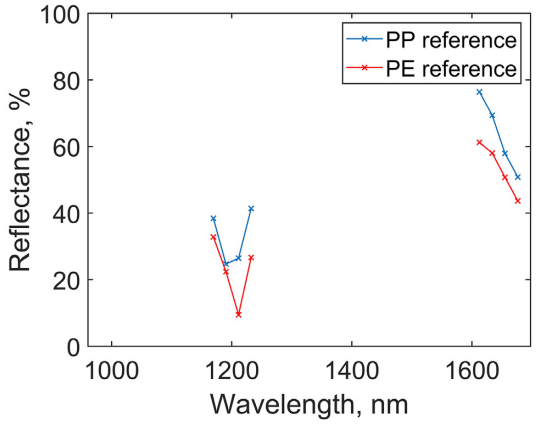

Figure 2. PE and PP reference spectra for spectral comparison of SWIR imagery of plastic items. Reference spectra represent a mean of spectra measured from eight PE items and seven PP items. Spectra are trimmed to exclude wavelengths impacted by noise caused by atmospheric absorption of IR or by detector sensitivity.

Hyperspectral band selection and noise reduction

The hyperspectral imager used in this study collects images in 36 SWIR bands, although many of these are impacted by atmospheric absorption, and noise dominates the imagery. In the collected data, eight bands (numbers 19–26) corresponding to wavelengths between 1337 and 1486 nm (1337.529, 1358.599, 1379.683, 1400.781, 1421.893, 1443.020, 1464.160, and 1485.315 nm) were consistently noisy. Bands 1 and 36 (corresponding to wavelengths 960.702 and 1697.645 nm), were also impacted by noise, owing to detector sensitivity limits. Of the remaining bands, eight within the ranges of 1169–1233 nm and 1612–1677 nm (bands 11–14 and 32–35, respectively) were selected for their relevance to characteristic absorption features of plastic, and these were used to perform spectral similarity calculations to detect plastic materials. Salt and pepper noise in the images collected in the selected bands was reduced with a 3 × 3-pixel median filter (applied to each band image) to remove small, sparse noise elements while preserving image detail.

Reference spectra construction

Multiple regions of interest (ROIs), all containing only plastic pixels, were manually delineated from each image of individual plastic items collected with the camera at waist height. The spectra of individual pixels within a given ROI were averaged to generate a spectrum representative of that ROI. Reference spectra for PE and PP—the two most abundant polymers in the natural environment—were constructed from the mean of all ROI spectra measured from items of these respective polymers.

Reference spectra for PE and PP are shown in Figure 2, where only the signal in the spectral bands relevant to plastic materials and minimally impacted by atmospheric absorp-

tion or other noise is considered. Both spectra exhibit distinct troughs at ~ 1200 nm and decreasing reflectance measured above 1600 nm with a local minimum in the 1677 nm band.

The mean spectra for the two distinct regions of the PE and PP reference spectra were calculated separately. The resulting averages were based on 11 and 12 spectra, respectively, for the 1200 and 1700 nm absorption features from images of eight PE items. For PP, the average spectral regions were based on 17 and 15 spectra, respectively, for 1200 and 1700 nm features from images of seven items. Multiple rectangular ROIs were delineated on some images to capture relevant signal, thus yielding more numerous spectra than items. Spectral segments inconsistent with the trend of the sample data and spectral data presented in the literature were disregarded and excluded from the calculation to preserve characteristic spectral features of the targeted materials (Masoumi *et al.*, 2012; Bogfjellmo, 2016; Zheng *et al.*, 2018; Zhu *et al.*, 2019; Garaba and Dierssen, 2020).

SAM and SCM

SAM is based on the cosine similarity [Equation (1)], which describes the similarity of two vectors by the angle between them (Kruse *et al.*, 1993). In this equation, A_i and B_i are the components of n-dimensional vectors A and B, separated by angle θ, in radians. The more similar the compared vectors, the smaller the value of θ.

$$\cos\theta = \frac{A \cdot B}{\|A\|\|B\|} = \frac{\sum_{i=1}^{n} A_i B_i}{\sqrt{\sum_{i=1}^{n} A_i^2}\sqrt{\sum_{i=1}^{n} B_i^2}}. \quad (1)$$

SCM centres vectors A_i and B_i by their respective means, $\bar{A}_i$ and $\bar{B}_i$, and captures negative correlation [Equation (2)]. Where results of SAM range between $\theta = 0°$ and 90°, results of SCM vary between $\theta = 0°$ and 180°.

$$\cos\theta = \frac{\sum_{i=1}^{n} \left(A_i - \bar{A}_i\right)\left(B_i - \bar{B}_i\right)}{\sqrt{\sum_{i=1}^{n} \left(A_i - \bar{A}_i\right)^2}\sqrt{\sum_{i=1}^{n} \left(B_i - \bar{B}_i\right)^2}}. \quad (2)$$

SCM was used to compare the trimmed spectrum (containing bands 11–14 and 32–35) of each pixel in a collected image to the reference spectra, to evaluate the similarity of each pixel's spectrum to each trimmed reference spectrum. Within this operation, each spectrum was mean-centred, to eliminate dissimilarities owing to differences in the absolute values of measured reflectance. The result, in radians, was converted to degrees. An 8-bit greyscale value for each pixel was assigned based on spectral angle, where the brightest pixels have the smallest spectral angles and the most similarity to the reference spectrum, and normalized to the range of 0–255 for each image.

Threshold selection

Histograms of pixel values from SCM analysis were visually inspected to determine an initial threshold value of similarity at which pixels were considered to contain the material represented by the reference spectrum. A typically bimodal distribution for images of individual plastic items corresponded to the plastic item (SCM angle close to zero) and background substrate (greater SCM angle). Applying a binary classification at this initial threshold value yielded maps classified into plastic (pixel value 1, white) and background substrate (pixel value 0, black).

For each reference spectrum and image containing the respective polymer (PE or PP), the threshold value (considering $\{\theta|\theta \in Z, 0° \leq \theta \leq 180°\}$) was refined by inspecting pixels outside the delineated plastic target area yet identified incorrectly as plastic. The purpose of this refinement is to minimize false positives in the application of the SCM algorithm, i.e. a conservative estimate. The mean threshold values (from nine images of PE and ten of PP) served as the thresholds to apply to aerial images of plastic items collected at a greater height, where the signal measured from the plastic was reduced, relative to the environmental background.

The MATLAB function, "imdilate" was used to expand white pixels considered to be plastic to assist visualization of the mapped results of threshold application—especially in the case of large composite images where the image resolution may exceed the display resolution and the disparity in resolution masks individual pixels. Each pixel considered to be plastic was expanded to also occupy the pixels surrounding it in a 5 × 5-pixel square, which formed the structuring parameter of the dilation.

Results

Examples of greyscale visible reference images and IR images used to manually delineate ROIs for reference spectra creation are shown in Figure 3, which depict a PE milk bottle and a PP margarine tub. Distorted spatial features in the IR band images are artefacts of stitching individual pushbroom scans together given inherently unsteady motion of the camera during image capture.

Histograms of SCM between pixels within images of individual plastic items to the selected reference spectrum revealed bimodal distributions (Figure 4). These distributions were used to determine the initial threshold value for clas-

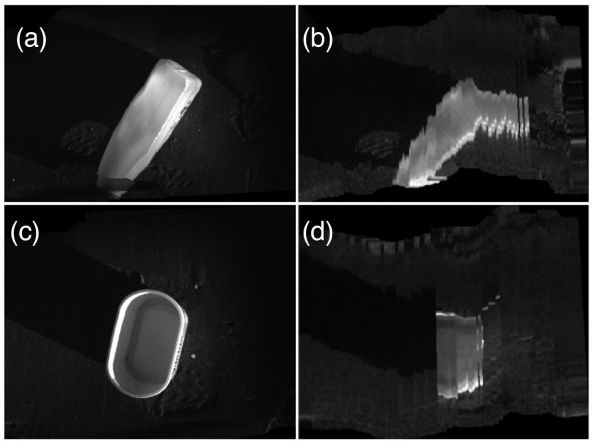

Figure 3. Reference images of a PE milk bottle (a) snapshot in the visible light regime and (b) pushbroom in the in the 1044.0 nm SWIR band, as well as a PP margarine tub (c) in the visible and (d) in the 1044.0 nm SWIR band. A 3 × 3-pixel median filter was applied to smooth images (b) and (d).

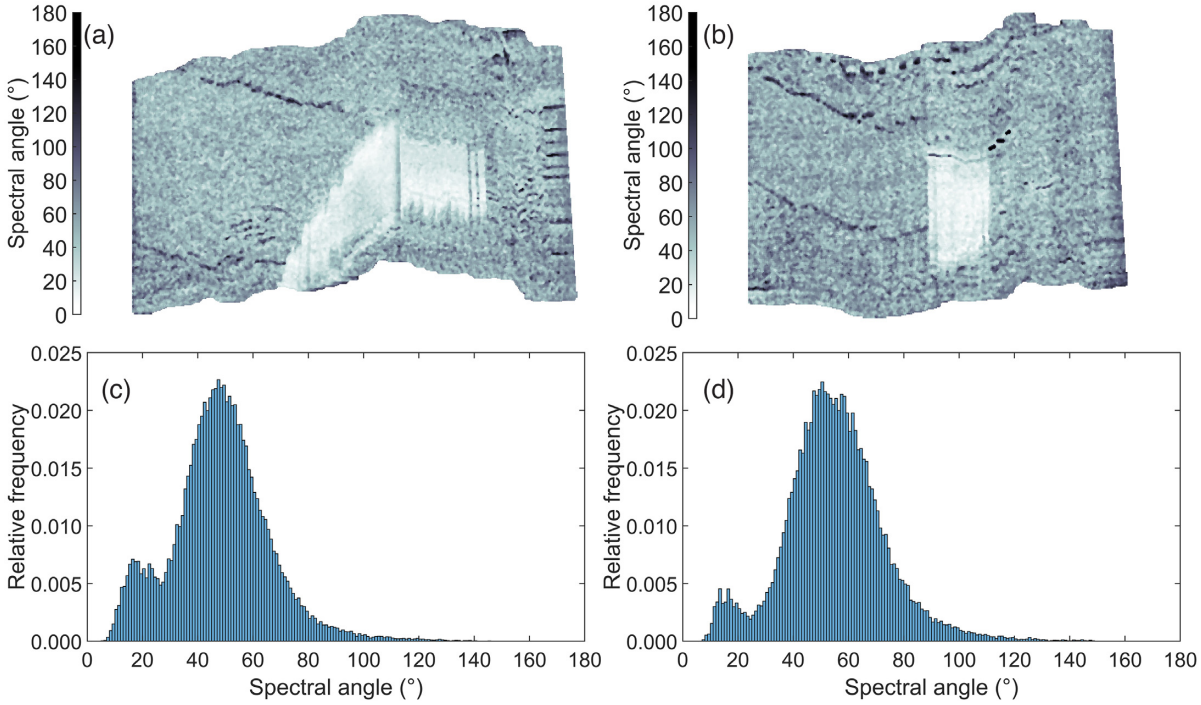

Figure 4. Results of spectral comparison by SCM algorithm of hyperspectral SWIR images of (a) PE milk bottle to a PE reference spectrum and (b) PP margarine tub to a PP reference spectrum. Colour scales in (a) and (b) range from 0° to 180° where lower values indicate greater spectral similarity and pixels are assigned greatest brightness. Histograms of pixel values in (a) and (b) appear in (c) and (d), respectively, indicating the proportions of pixels with given spectral angle values, in degrees.

sifying plastic and non-plastic material. The mean threshold value, after refining to yield no false positive pixels (as described in "Methods") was 17° for PE items as well as PP items. Detection of plastic items can be visualized by applying the selected threshold to the SCM image (Figure 5). Since the selected threshold is a mean value instead of the most conservative and minimum threshold value observed for a single image, some individual classified images contain false positive pixel detections after applying the mean threshold.

Aerial transects of the preliminary and environmentally sourced assortments of plastic are shown in Figures 6 and 7. Plastic items are observable by eye in the 1044.0 nm SWIR band shown, and SCM results highlight pixels classified as plastic based on a 17° similarity to the PE and PP reference spectra. Several plastic items were detected at this threshold in each scenario that compares the pixels within each transect to each of the reference spectra. In each of these combinations, the SCM application detected plastic items that match the polymer type of the reference spectrum, as well as other items of different polymer types. Detection sensitivity was explored as a function of classification threshold for values between $\theta = 16°$ and $\theta = 20°$, at 1° intervals. A true detection was considered as the presence of at least one white pixel in a region estimated to be spatially correlated to a plastic item by visual inspection and pixel position comparison. A summary of total detected items, as well as PE and PP items detected with the respective reference spectra are quantified in Table 3 (detailed detection results are provided in Supplementary Tables S1 and S2). The resulting proportions of items positively detected are shown in Figure 8.

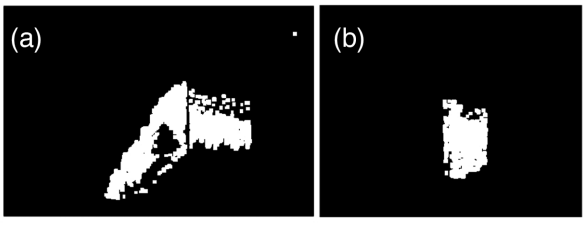

Figure 5. SWIR imagery of (a) PE milk bottle and (b) PP margarine tub on a beach, with pixels classified as the respective polymer (white), by SCM with a classification threshold of 17°.

Spectral comparison of image pixels to the PP reference spectrum, rather than PE reference spectrum, consistently resulted in more items being detected within both item assortments, and across varying spectral angle thresholds. In the preliminary assortment, the percentage of total items detected ranged between 15 and 33% for the PE reference and 30 and 56% for the PP reference. The detection rates for PP items (60–80%) were consistently at least twice as great as for PE items (20–40%) when comparing pixels to the respective reference spectra. Spectral comparison to the PP reference also detected all but one of the PET bottles within the assortment (at the least conservative threshold value tested and all bottles having a label on at least one side). Only PE and PP items and PET items with labels, but no other types of resins, were detected within the preliminary assortment. Spectral comparisons to the PE and PP reference spec-

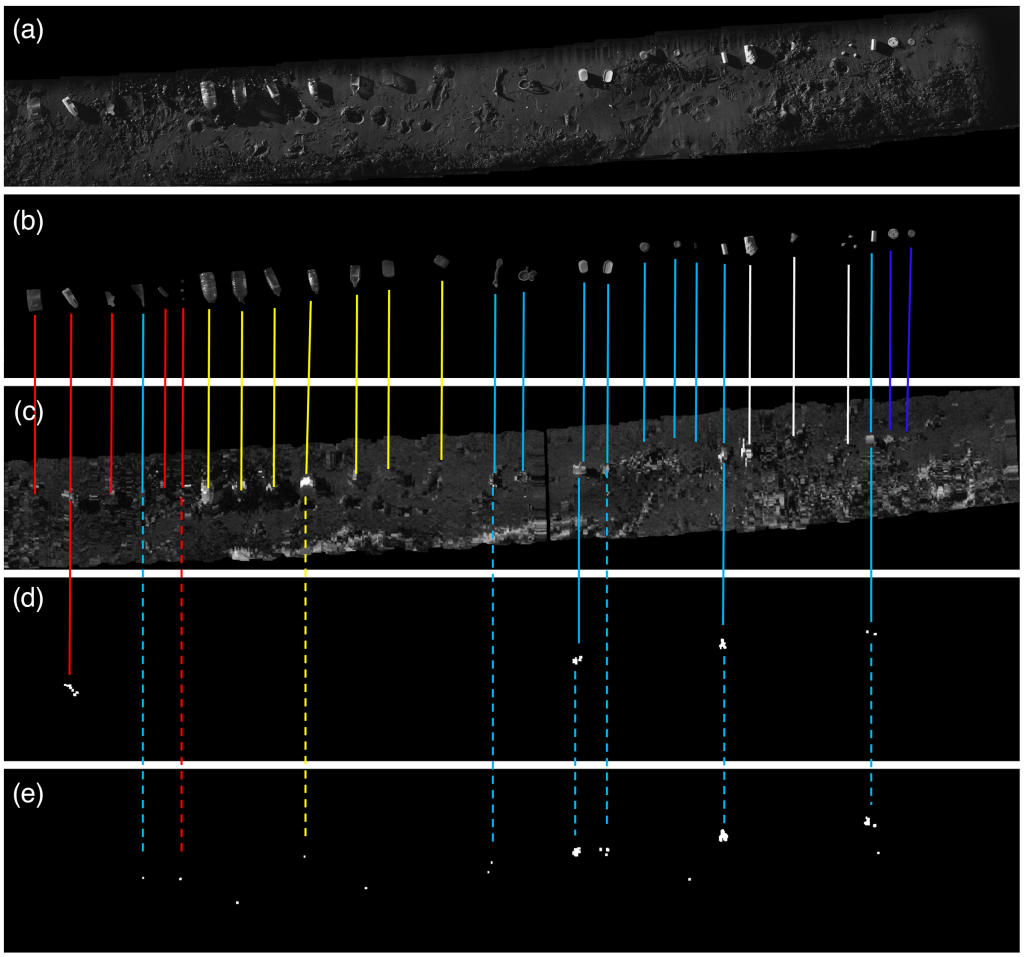

Figure 6. (a) Visible reference image of plastic items in the preliminary assortment; (b) image "a" masked to highlight placed items; (c) IR image of the scene in in the 1044.0 nm band (3 × 3-pixel median filter applied for smoothing); pixels classified as plastic by the SCM algorithm based on a 17° similarity to (d) a PE reference spectrum (solid lines between "c" and "d") and (e) a PP reference spectrum (dashed lines between "c" and "e" or between "d" and "e"). In order of resin code, PET items are denoted by yellow lines, PE by red, PP by blue, EPS by grey, and "other" by indigo.

tra each yielded detections of the other polymer—between 30 and 60% of the PP items (three to six out of ten) detected with the PE reference and between 20 and 60% of the PE items (one to three out of five) detected with the PP reference. In consideration of this overlap, combining the results of the two spectral comparisons (total items detected with either of the reference spectra) provided increases in detection rates relative to detection rates based on individual spectral comparisons. These increases were greater relative to PE reference comparisons and modest relative to PP reference comparisons.

None of the seven PET bottles (regardless of transparency and fouling) in the environmentally sourced assortment were detected within the applied thresholds for either reference, including the only bottle with a label. The opaque PET drinking pouch was detected with both references. Spectral comparison with the PE reference detected one of three PVC items, whereas the PP reference detected all three. The PP reference also detected three of four PS items while the PE reference detected just one (at thresholds greater than 17°). The preliminary assortment does not contain PVC and PS items—the collection was harvested primarily from recycling and neither PVC nor PS are commonly recycled. Both PE and PP references detected the nylon 6 bag. All four PE/PP blend items were detected by both references at at least one applied threshold value. Black items (an HDPE barrel lid, an HDPE fragment, and a melamine ash tray) were not detected with either reference at any tested threshold value.

Detection rate as a percentage of the total items within an assortment increases with spectral angle threshold for the selected threshold values. As the threshold value increases, however, so do false positives, i.e. non-plastic pixels erroneously classified as plastic. At greater threshold values, false positives become so numerous that their quantity and scattered distribution compromise reliable, manual matching of highlighted pixels to true plastic items in the visible and IR reference images. For this reason, plastic items were counted for a lower range of threshold values for the comparison of the environmentally sourced assortment transect to the PP reference spectrum. Detection rates among the environmentally sourced assortment are consistently greater than those attained from the preliminary assortment.

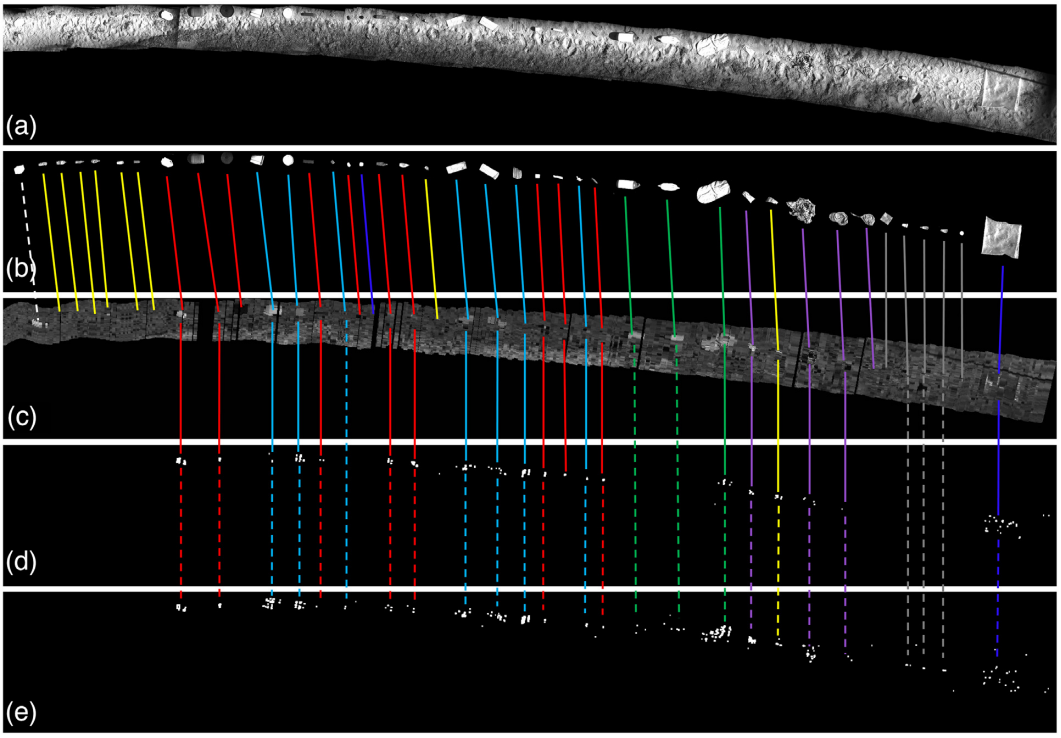

Figure 7. (a) Visible reference image of plastic items in an environmentally sourced assortment; (b) image "a" masked to highlight placed items; (c) IR image of the scene in the 1044.0 nm band (3 × 3-pixel median filter applied for smoothing); pixels classified as plastic by the SCM algorithm based on a 17° similarity to (d) a PE reference spectrum (solid lines between "c" and "d") and (e) a PP reference spectrum (dashed lines between "c" and "e" or between "d" and "e"). In order of resin code, PET items are denoted by yellow lines, PE by red, PVC by green, PP by blue, PS by grey, PE/PP blend by violet, and "other" by indigo. Note that the white dashed line between panels "b" and "c" indicates the location of a paper white reference.

Table 3. Plastic items detected by SCM algorithm and manually counted in SWIR imagery transects of preliminary and environmentally sourced assortments of plastic items on a beach, with respect to a PE and PP reference spectrum, where classification threshold is specified by spectral angle (°). Greater threshold values increase true positive detections, as well as false positive pixel classifications. Classification and counting were performed at a lower range of threshold values for the comparison of the environmentally sourced transect to the PP reference due to an abundance of false positives at 19° and greater.

		SCM threshold	16°	17°	18°	19°	20°
Preliminary assortment	PE reference	Of 27 total items	– –	4 15%	5 19%	8 30%	9 33%
		Of 5 PE items	– –	1 20%	1 20%	2 40%	2 40%
	PP reference	Of 27 total items	– –	8 30%	11 41%	12 44%	15 56%
		Of 10 PP items	– –	6 60%	8 80%	8 80%	8 80%
	Either PE or PP reference	Of 27 total items	– –	9 33%	12 44%	14 52%	17 63%
Environmentally sourced assortment	PE reference	Of 39 total items	– –	20 51%	21 54%	22 56%	22 56%
		Of 14 PE and PE blend items	– –	11 79%	11 79%	12 86%	12 86%
	PP reference	Of 39 total items	23 59%	25 64%	27 69%	– –	– –
		Of 11 PP and PP blend items	10 91%	10 91%	11 100%	– –	– –
	Either PE or PP reference	Of 39 total items	– –	26 67%	27 69%	– –	– –

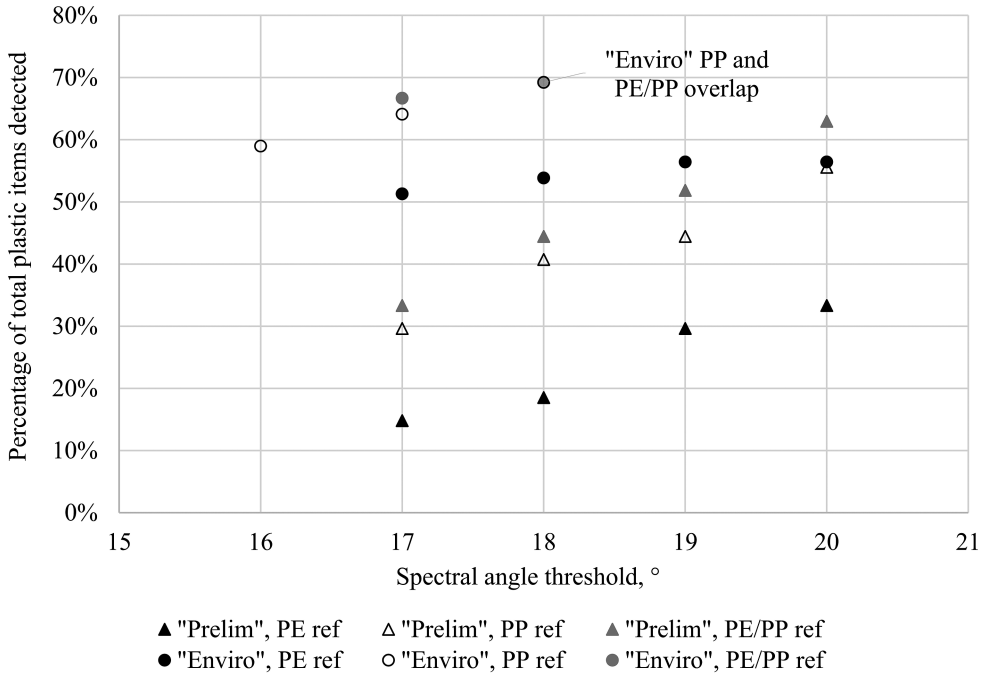

Figure 8. Percentage of total plastic items in preliminary ("prelim"; triangles) and environmentally sourced ("enviro"; circles) assortments detected on a beach by spectral angle comparison of SWIR imagery to PE (solid black markers) and PP (open markers) reference spectra, and to either of these reference spectra (solid grey markers).

Discussion

This study establishes the viability of detecting beached marine plastics in a natural, shoreline environment with hyperspectral SWIR imaging deployed at below-cloud altitude. Positive detections of assorted plastic items were achieved through the application of an SCM algorithm, comparing image spectra to PE and PP reference spectra, within a spectral similarity threshold range of 16–20°.

Distinct contrast between the reflectance of plastic items and their terrestrial surroundings in the captured SWIR imagery supports the viability of the technology as a tool for detection of plastic debris under natural sunlight. In this study, the identified absorption features at ~1200 and ~1700 nm in the measured spectra of PE and PP items are consistent with those observed in other SWIR characterization studies of plastic materials (Masoumi *et al.*, 2012; Bogfjellmo, 2016; Zheng *et al.*, 2018; Zhu *et al.*, 2019; Garaba and Dierssen, 2020).

The mapped results of applying the SCM algorithm to the SWIR imagery collected at waist height, and spectrally compared to the absorption features of the PE and PP reference spectra, also yields contrast between the plastic and surroundings that is discernible visually and by inspection of the image histograms. The selected threshold of $\theta = 17°$ for classifying pixels as "similar" to plastic with SCM aligns reasonably with thresholds reported in the literature regarding similar applications, using the SAM algorithm. An investigative, rather than direct comparison is made here because SCM accounts for negative correlations and is defined over the range of 0–180° whereas SAM results are defined by the range of 0–90°. Garaba and Dierssen (2018) created a discrete scale to describe the spectral similarity of marine-harvested macroplastics to one another: very strong ($0° \leq \theta \leq 5°$), strong ($5° < \theta \leq 10°$), moderate ($10° < \theta \leq 15°$), weak ($15° < \theta \leq 20°$), and very weak ($\theta > 20°$). While Garaba and Dierssen (2018) compared individual beached macroplastics to one another, our study compares the spectra of a variety of domestic and environmentally sourced plastic items to mean reference spectra also based on a collection of multiple items from the same, varied sources. The increased diversity of targets may account for the greater, less conservative angle yielded as a classification threshold in our study.

Further, Garaba and Dierssen (2018) measured spectra with a spectroradiometer over a greater spectral range and with greater spectral resolution (350–2500 nm interpolated to a 1 nm resolution) than the BaySpec imager offers. SAM was applied in a piecewise approach to compare spectra within individual SWIR regions that capture absorption features: 905–955, 1160–1260, 1380–1480, and 1715–1750 nm. The maximum spectral angle reported within these ranges was 10.5°. Our study simultaneously compares spectra between 1169–1233 and 1612–1677 nm with just four measured data points within each region. The potential for discrepancy between spectra increases with greater spectral range considered. Garaba and Dierssen (2018) reported that over the full 350–2500 nm range that includes visible light (acknowledging that item colour influences spectral characteristics), the range of spectral similarity for macroplastics was 5.7–38.2° with a mean of 19.1°—a weaker similarity than yielded by piecewise comparisons. Garaba and Dierssen (2018) additionally point to SAM thresholds of $\theta = 17.2°$ and $\theta = 11.5°$ used, in land use and coral mapping hyperspectral imagery studies, respectively (Kutser *et al.*, 2006; Petropoulos *et al.*, 2013).

Detection of the plastic sample items used in this study did not appear to be compromised by the items' exposure to the natural environment, relative to detection of items harvested from recycling. Greater proportions of total plastic items, as well as specifically PE and PP items, were detected with each reference spectrum in the environmentally sourced

assortment, against the preliminary assortment. PE, PP, and PE/PP blend items comprised 54% of the items in both assortments. Only PET items with labels were detected in the preliminary assortment, and those without were not detected in either assortment (except for the opaque drinking pouch with no fouling). Based on this result, PET materials are not likely to be detected by spectral comparison to PE and PP reference spectra. No other resins were detected in the preliminary assortment. Masoumi *et al.* (2012) demonstrated that the spectral characteristics of PET differ noticeably from those of PE and PP within the spectral regions compared here and Balsi *et al.* (2021) specifically emphasized the spectral differences between PET and PE. The spectral characteristics of PVC and PS bear more similarity (by visual inspection) to those of PE and especially to those of PP (Masoumi *et al.*, 2012). The local maximum absorption in the ~ 1200 nm region occurs at a greater wavelength for PE than PP, PVC, and PS in the Masoumi *et al.* (2012) data and the same observation is made in the PE and PP reference spectra generated in this study. The greater similarity between PP, PVC, and PS spectral characteristics supports the greater detection rates of plastic items achieved with the PP reference spectrum than with the PE reference spectrum. Balsi *et al.* (2021) noted that PP items were classified as PE or as both PE and PET in aerial surveys due to PP's spectral similarity to these other polymers.

In addition to PE and PP, PVC, and PS items were detected in the environmentally sourced assortment and the nylon 6 item was detected in each reference/threshold combination. These three additional resins comprise another 23% of the environmentally sourced items. Considering PE and PP (and their blends), PVC, PS, and nylon 6 as probable detectable materials by spectral comparison to PE and PP spectra, the proportions of such items are 54% and 74%, respectively, in the preliminary and environmentally sourced assortments. This difference in resin proportions can account for discrepancy in total detection rates between the two assortments. Items with surface contamination in the environmentally sourced assortment were detected despite this fouling. Masoumi *et al.* (2012) demonstrated strong similarity between spectra of clean items and items with a contamination layer thinner than 0.5 mm, for a given plastic type. These results directly support the feasibility of detecting shoreline plastic debris by RS and the analysis methods presented in this study.

Transparent PET evidently presents a challenge for reliable detection of this material. Bogfjellmo (2016) reported that pixels containing transparent PET were influenced by background spectra and remained unclassified by SAM within SWIR imagery captured indoors on a glass background. PE, PP, PVC, and PS samples were reliably classified under the same conditions, as were white fragments of PET on a black cardboard background. Positive detections with the PP reference spectrum of transparent PET items in the present study correspond to bottles partially covered with labels. This result suggests that the labels may be comprised of PP, and responsible for the spectral similarity to the PP reference. A 2-L bottle with a label was, however, not detected within the environmentally sourced assortment of plastics. The absence of labels on all but one of the bottles (including PET and HDPE) in the environmentally sourced assortment is likely due to environmental factors such as UV exposure and wave action that may weaken adhesive and mechanically remove labels. Masoumi *et al.* (2012) were able to optically sort PET bottles (from HDPE, PVC, PP, and PS items) that were covered up to 35% by a label, under controlled illumination with a measure of relative reflectance, specifically tailored to an absorption feature characteristic of PET. The application of such an approach, or comparison with SCM to a PET-specific reference spectrum may aid detection of PET items in the environment; however, the influence of background spectra remains a consideration for transparent items. The positive detection of the opaque, reusable drinking pouch, and the negative detection of the opaque, purple drinking bottle in this study may be due to the smaller size of the latter, contributing less signal within the scene.

Black plastics were not detected, which is consistent with the limitation within the recycling industry to sort black materials with SWIR technology due to the black pigment's strong absorption and low reflectance of IR energy (Masoumi *et al.*, 2012; Kassouf *et al.*, 2014; Bogfjellmo, 2016). Only the environmental assortment contained black plastic items. Of the three of these, one was melamine and the others PE. Presuming it is not possible to detect black plastics with SWIR instrumentation, the maximum possible detection rate was 92% (36/39) for total items and 80% (8/10) for PE items.

There is no evident correlation in the collected and analysed data regarding the location of false positive detections. False positive pixels appear at greater threshold values in the images collected at waist height of individual items on a relatively uniform sand background, as well as in the longer, stitched transect mosaics whose backgrounds are more varied and include seaweed debris.

We observed gaps and distortions in the stitched pushbroom images presented here, which could be addressed with an active stabilization solution to counter the motion and vibration of a necessarily mobile platform and to increase image and data quality. Petrie (2005) indicates that pushbroom instruments must be operated from a stable platform and that changes in instrument altitude and attitude will otherwise produce gaps and double imaging in the collected imagery. The manufacturer's documentation for the BaySpec instrument specifies the necessity of a gimbal for UAV applications to keep the lens of the imager perpendicular to the scene below. Further, Turner *et al.* (2017) indicate that mounting a pushbroom imager on a gimbal can reduce the impact of aerial platform movement and Sigernes *et al.* (2018) demonstrate successful imaging campaigns with bespoke hyperspectral pushbroom imagers stabilized by commercial, off-the-shelf gimbals in both handheld and UAV-based operations.

This study focused on shoreline, rather than floating plastics because pushbroom imagery is better suited to scenes with discernible, stationary features as spatial references with which to stitch individual images together. Balsi *et al.* (2021) addressed this challenge associated with pushbroom imagery with a real-time detection solution that uses a computationally efficient Linear Discriminant Analysis, which does not rely upon post-processed, mosaic imagery. SCM also has low computational requirements and may also be suitable for real-time detection applications.

Deploying the SWIR imaging technology on a UAV would allow for evaluation of the impact of altitude, towards determining a limit of detection for plastic items of a given size or type. The flexibility of such an aerial platform would also support deployment of the imager at a variety of sites and with different terrain and environmental background, e.g. sand, rock, kelp detritus, and snow and ice. Melvin *et al.* (2021) discuss the importance of considering a greater variety of shore-

line environments in plastic pollution research, as landscape features such as sediment grain size, accumulated organic material, and winter precipitation may affect how plastic materials are deposited on the shoreline. As discussed by Arroyo-Mora *et al.* (2021) regarding vegetation-focused RS applications, analysis of data collected under different cloud coverage is needed to investigate the method's performance especially under diffuse illumination when less natural light might be available, relative to a clear sky.

Conclusion

This study demonstrates that hyperspectral SWIR imaging and SCM can be applied to successfully detect plastic as a broad material class, including the most abundant types of plastic debris (PE and PP) and additional polymers in a sandy shoreline environment. As different polymers are characterized by different spectral features (Balsi *et al.*, 2021), further comparisons to reference spectra specific to other types of plastic (e.g. PET, PVC, and PS) could support more reliable detection of these distinct types of plastic.

The detection performance of the technology could be compared in practical application to clean-up methods, by capturing and analysing the imagery of a beach before and after a clean-up, where visual observations and data recorded by volunteers serve as the ground truth. Simultaneous capture of aerial RGB imagery could support the verification of any true detections in the SWIR imagery not verified directly by the volunteers' observations.

Funding

This work has been completed within the NEXUSS Centre for Doctoral Training granted by the UK Natural Environment Research Council (NERC) (grant number NE/R012156/1, studentship 1971900).

Supplementary data

Supplementary material is available at the *ICESJMS* online version of the manuscript.

Data availability statement

The data underlying this article are available in the article and in its online supplementary material.

Acknowledgements

The authors thank Reidar Kaasa for providing valuable assistance in setting up and supporting the highline fieldwork experiments and Janie Steele for providing beach-harvested plastic items. The constructive comments from anonymous reviewers of an earlier version of this manuscript are gratefully acknowledged.

References

Acuña-Ruz, T., Uribe, D., Taylor, R., Amézquita, L., Guzmán, M.C., Merrill, J., Martínez, P. *et al.* 2018. Anthropogenic marine debris over beaches: spectral characterization for remote sensing applications. Remote Sensing of Environment, 217: 309–322. Elsevier.

Andrady, A.L. 2011. Microplastics in the marine environment. Marine Pollution Bulletin, 62: 1596–1605. Elsevier.

Andriolo, U., Gonçalves, G., Rangel-Buitrago, N., Paterni, M., Bessa, F., Gonçalves, L.M., Sobral, P. *et al.* 2021a. Drones for litter mapping: an inter-operator concordance test in marking beached items on aerial images. Marine Pollution Bulletin, 169: 112542. Elsevier.

Andriolo, U., Gonçalves, G., Sobral, P., and Bessa, F. 2021b. Spatial and size distribution of macro-litter on coastal dunes from drone images: a case study on the atlantic coast. Marine Pollution Bulletin, 169: 112490. Elsevier.

Arroyo-Mora, J.P., Kalacska, M., Løke, T., Schläpfer, D., Coops, N.C., Lucanus, O., and Leblanc, G. 2021. Assessing the impact of illumination on UAV pushbroom hyperspectral imagery collected under various cloud cover conditions. Remote Sensing of Environment, 258: 112396. Elsevier.

Avio, C.G., Gorbi, S., and Regoli, F. 2017. Plastics and microplastics in the oceans: from emerging pollutants to emerged threat. Marine Environmental Research, 128: 2–11. Elsevier.

Balsi, M., Moroni, M., Chiarabini, V., and Tanda, G. 2021. High-resolution aerial detection of marine plastic litter by hyperspectral sensing. Remote Sensing, 13: 1557. Multidisciplinary Digital Publishing Institute.

Biermann, L., Clewley, D., Martinez-Vicente, V., and Topouzelis, K. 2020. Finding plastic patches in coastal waters using optical satellite data. Scientific Reports, 10: 1–10. Nature Publishing Group.

Bogfjellmo, S. 2016. Hyperspectral analysis of plastic particles in the ocean. Masters thesis, Norwegian University of Science and Technology, Trondheim, Norway.

Boucher, J., and Billard, G. 2019. The challenges of measuring plastic pollution. Field actions science reports. The Journal of Field Actions, Special Issue 19:68–75. Institut Veolia.

Cincinelli, A., Scopetani, C., Chelazzi, D., Lombardini, E., Martellini, T., Katsoyiannis, A., Fossi, M.C. *et al.* 2017. Microplastic in the surface waters of the Ross Sea (Antarctica): occurrence, distribution and characterization by FTIR. Chemosphere, 175: 391–400.

CONTAM. 2016. Presence of microplastics and nanoplastics in food, with particular focus on seafood. EFSA Journal, 14: e04501. Wiley Online Library.

De Carvalho, O.A., and Meneses, P.R. 2000. Spectral correlation mapper (SCM): an improvement on the spectral angle mapper (SAM). *In* Summaries of the Ninth JPL Airborne Earth Science Workshop, JPL Publication, 00–18.

Duarte, D., Andriolo, U., and Gonçalves, G. 2020. Addressing the class imbalance problem in the automatic image classification of coastal litter from orthophotos derived from UAS imagery. ISPRS Annals of the Photogrammetry, Remote Sensing and Spatial Information Sciences, 3: 439–445. Copernicus GmbH.

Freitas, S., Silva, H., and Silva, E. 2021. Remote hyperspectral imaging acquisition and characterization for marine litter detection. Remote Sensing, 13: 2536. Multidisciplinary Digital Publishing Institute.

Gall, S.C., and Thompson, R.C. 2015. The impact of debris on marine life. Marine Pollution Bulletin, 92: 170–179. Elsevier.

Garaba, S.P., Aitken, J., Slat, B., Dierssen, H.M., Lebreton, L., Zielinski, O., and Reisser, J. 2018. Sensing ocean plastics with an airborne hyperspectral shortwave infrared imager. Environmental Science and Technology, 52: 11699–11707. ACS Publications.

Garaba, S.P., and Dierssen, H.M. 2018. An airborne remote sensing case study of synthetic hydrocarbon detection using short wave infrared absorption features identified from marine-harvested macro-and microplastics. Remote Sensing of Environment, 205: 224–235. Elsevier.

Garaba, S.P., and Dierssen, H.M. 2020. Hyperspectral ultraviolet to shortwave infrared characteristics of marine-harvested, washed-ashore and virgin plastics. Earth System Science Data, 12: 77–86. Copernicus GmbH.

GESAMP. 2015. Sources, fate and effects of microplastics in the marine environment: a global assessment. (IMO/FAO/UNESCO-IOC/UNIDO/WMO/IAEA/UN/UNEP/UNDP joint group of experts

on the scientific aspects of marine environmental protection). Reports and Studies GESAMP No 90. International Maritime Organization, London. p. 96.

Goddijn-Murphy, L., and Dufaur, J. 2018. Proof of concept for a model of light reflectance of plastics floating on natural waters. Marine Pollution Bulletin, 135: 1145–1157.

Goddijn-Murphy, L., and Williamson, B. 2019. On thermal infrared remote sensing of plastic pollution in natural waters. Remote Sensing, 11: 2159. Multidisciplinary Digital Publishing Institute.

Guffogg, J.A., Soto-Berelov, M., Jones, S.D., Bellman, C.J., Lavers, J.L., and Skidmore, A.K. 2021. Towards the spectral mapping of plastic debris on beaches. Remote Sensing, 13: 1850. Multidisciplinary Digital Publishing Institute.

Jambeck, J.R., Geyer, R., Wilcox, C., Siegler, T.R., Perryman, M., Andrady, A., Narayan, R. *et al.* 2015. Plastic waste inputs from land into the ocean. Science, 347: 768–771. American Association for the Advancement of Science.

Kassouf, A., Maalouly, J., Rutledge, D.N., Chebib, H., and Ducruet, V. 2014. Rapid discrimination of plastic packaging materials using MIR spectroscopy coupled with independent components analysis (ICA). Waste Management, 34: 2131–2138.

Kershaw, P., Turra, A., and Galgani, F. 2019. Guidelines for the monitoring and assessment of plastic litter in the ocean. GESAMP Reports and Studies No 99. GESAMP.

Kruse, F.A., Lefkoff, A., Boardman, J., Heidebrecht, K., Shapiro, A., Barloon, P., and Goetz, A. 1993. The spectral image processing system (SIPS)—interactive visualization and analysis of imaging spectrometer data. Remote Sensing of Environment, 44: 145–163. Elsevier.

Kulcke, A., Gurschler, C., Spöck, G., Leitner, R., and Kraft, M. 2003. On-line classification of synthetic polymers using near infrared spectral imaging. Journal of Near Infrared Spectroscopy, 11: 71–81. SAGE Publishing.

Kutser, T., Miller, I., and Jupp, D.L. 2006. Mapping coral reef benthic substrates using hyperspectral space-borne images and spectral libraries. Estuarine, Coastal and Shelf Science, 70: 449–460. Elsevier.

Law, K.L., Morét-Ferguson, S.E., Goodwin, D.S., Zettler, E.R., Deforce, E., Kukulka, T., and Proskurowski, G. 2014. Distribution of surface plastic debris in the eastern Pacific Ocean from an 11-year data set. Environmental Science and Technology, 48: 4732–4738.

Law, K.L., Starr, N., Siegler, T.R., Jambeck, J.R., Mallos, N.J., and Leonard, G.H. 2020. The United States' contribution of plastic waste to land and ocean. Science Advances, 6: eabd0288. American Association for the Advancement of Science.

Lebreton, L., Egger, M., and Slat, B. 2019. A global mass budget for positively buoyant macroplastic debris in the ocean. Scientific Reports, 9: 1–10. Nature Publishing Group.

Mace, T.H. 2012. At-sea detection of marine debris: overview of technologies, processes, issues, and options. Marine Pollution Bulletin, 65: 23–27.

Mai, L., Bao, L.-J., Shi, L., Wong, C.S., and Zeng, E.Y. 2018. A review of methods for measuring microplastics in aquatic environments. Environmental Science and Pollution Research, 25: 11319–11332. Springer.

Martinez-Vicente, V., Clark, J.R., Corradi, P., Aliani, S., Arias, M., Bochow, M., Bonnery, G. *et al.* 2019. Measuring marine plastic debris from space: initial assessment of observation requirements. Remote Sensing, 11: 2443. Multidisciplinary Digital Publishing Institute.

Masoumi, H., Safavi, S.M., and Khani, Z. 2012. Identification and classification of plastic resins using near infrared reflectance. International Journal of Mechanical, Aerospace, Industrial, Mechatronic and Manufacturing Engineering, 6: 213–220.

Melvin, J., Bury, M., Ammendolia, J., Mather, C., and Liboiron, M. 2021. Critical gaps in shoreline plastics pollution research. Frontiers in Marine Science, 8: 845. Frontiers.

Peckham, J., O'Young, S., and Jacobs, J.T. 2015. Comparison of medium and long wave infrared imaging for ocean based sensing. Journal of Ocean Technology, 10:112–128.

Petrie, G. 2005. Airborne pushbroom line scanners: an alternative to digital frame scanners. GeoInformatics, 8: 50–57.

Petropoulos, G.P., Vadrevu, K.P., and Kalaitzidis, C. 2013. Spectral angle mapper and object-based classification combined with hyperspectral remote sensing imagery for obtaining land use/cover mapping in a mediterranean region. Geocarto International, 28: 114–129. Taylor & Francis.

Phillips, R.A., and Waluda, C.M. 2020. Albatrosses and petrels at South Georgia as sentinels of marine debris input from vessels in the southwest Atlantic Ocean. Environment International, 136: 105443. Elsevier.

Renner, G., Schmidt, T.C., and Schram, J. 2017a. Characterization and quantification of microplastics by infrared spectroscopy. *In* Comprehensive Analytical Chemistry, pp. 67–118. Elsevier.

Renner, G., Schmidt, T.C., and Schram, J. 2017b. A new chemometric approach for automatic identification of microplastics from environmental compartments based on FT-IR spectroscopy. Analytical Chemistry, 89: 12045–12053.

Shivakumar, B., and Rajashekararadhya, S. 2017. Performance evaluation of spectral angle mapper and spectral correlation mapper classifiers over multiple remote sensor data. *In* Proceedings of the 2017 Second International Conference on Electrical, Computer and Communication Technologies (ICECCT), pp. 1–6. IEEE, Coimbatore, India.

Sigernes, F., Syrjäsuo, M., Storvold, R., Fortuna, J., Grøtte, M.E., and Johansen, T.A. 2018. Do it yourself hyperspectral imager for handheld to airborne operations. Optics Express, 26: 6021–6035. Optical Society of America.

Ter Halle, A., Ladirat, L., Martignac, M., Mingotaud, A.F., Boyron, O., and Perez, E. 2017. To what extent are microplastics from the open ocean weathered? Environmental Pollution, 227: 167–174. Elsevier.

Turner, D., Lucieer, A., McCabe, M., Parkes, S., and Clarke, I. 2017. Pushbroom hyperspectral imaging from an unmanned aircraft system (UAS)-geometric processing workflow and accuracy assessment. *In* International Archives of the Photogrammetry, Remote Sensing and Spatial information. Copernicus GmbH, Germany. pp. 379–384.

Van Franeker, J.A., and Law, K.L. 2015. Seabirds, gyres and global trends in plastic pollution. Environmental Pollution, 203: 89–96. Elsevier.

Veenstra, T.S., and Churnside, J.H. 2012. Airborne sensors for detecting large marine debris at sea. Marine Pollution Bulletin, 65: 63–68. Elsevier Ltd.

Waller, C.L., Griffiths, H.J., Waluda, C.M., Thorpe, S.E., Loaiza, I., Moreno, B., Pacherres, C.O. *et al.* 2017. Microplastics in the Antarctic marine system: an emerging area of research. The Science of the Total Environment, 598: 220–227.

Zheng, Y., Bai, J., Xu, J., Li, X., and Zhang, Y. 2018. A discrimination model in waste plastics sorting using NIR hyperspectral imaging system. Waste Management, 72: 87–98. Elsevier.

Zhu, S., Chen, H., Wang, M., Guo, X., Lei, Y., and Jin, G. 2019. Plastic solid waste identification system based on near infrared spectroscopy in combination with support vector machine. Advanced Industrial and Engineering Polymer Research, 2: 77–81. Elsevier.

Handling Editor: Juan Bellas